

Recent Applications of Higher-Order Spectral Analysis to Nonlinear Aeroelastic Phenomena

Walter A. Silva*

NASA Langley Research Center, Hampton, Virginia, 23681

Muhammad R. Hajj†

Virginia Polytechnic Institute and State University, Blacksburg, Virginia

Shane Dunn‡

Defence Science and Technology Organisation, Department of Defence, Australia

Thomas W. Strganac§

Edward J. Powers¶

Texas A&M University, College Station, Texas

University of Texas at Austin, Austin, Texas

Ronald Stearman||

University of Texas at Austin, Austin, Texas

Recent applications of higher-order spectral (HOS) methods to nonlinear aeroelastic phenomena are presented. Applications include the analysis of data from a simulated nonlinear pitch and plunge apparatus and from F-18 flight flutter tests. A MATLAB model of the Texas A&M University's Nonlinear Aeroelastic Testbed Apparatus (NATA) is used to generate aeroelastic transients at various conditions including limit cycle oscillations (LCO). The Gaussian or non-Gaussian nature of the transients is investigated, related to HOS methods, and used to identify levels of increasing nonlinear aeroelastic response. Royal Australian Air Force (RAAF) F/A-18 flight flutter test data is presented and analyzed. The data includes high-quality measurements of forced responses and LCO phenomena. Standard power spectral density (PSD) techniques and HOS methods are applied to the data and presented. The goal of this research is to develop methods that can identify the onset of nonlinear aeroelastic phenomena, such as LCO, during flutter testing.

Introduction

The study of nonlinear aeroelastic phenomena, in particular that of limit cycle oscillations (LCO), has become an important field of study in recent years.¹ A major motivating factor for this increased interest is the fact that several operational aircraft continue to experience LCO within their flight envelope, often leading to a flight restriction or performance degradation.^{2,3} Several researchers have been using the Nonlinear Aeroelastic Testbed Apparatus (NATA) at Texas A&M University's Low-Speed Wind Tunnel to investigate fundamental aspects of LCO behavior,⁴⁻⁹ including application of higher-order spectral methods to the identification of nonlinear aeroelastic phenomena.¹⁰

An aeroelastic LCO is the result of nonlinear dynamics in the structural system or the aerodynamic system, or both. Quite often, as the amplitude of an initial flutter incident increases, the nonlinearities associated with the aeroelastic system become significant. As these nonlinearities grow in magnitude, the

*Senior Research Scientist, Aeroelasticity Branch, AIAA Associate Fellow.

†Professor, Engineering Science and Mechanics.

‡Head-Aeroelasticity, Air Vehicles Division.

§Associate Professor, Department of Aerospace Engineering, AIAA Associate Fellow.

¶Professor, Department of Electrical Engineering.

||Professor, Department of Aerospace Engineering.

aeroelastic system is transformed from an initially unstable linear flutter event into a limited amplitude nonlinear aeroelastic oscillation, or an LCO. Denegri³ discusses the different types of LCO encountered by the F-16 aircraft during its flight flutter testing phase.

Recently, higher-order spectral methods have been applied to experimental flutter measurements from wind-tunnel data¹¹ and flight test data.¹² Analyses using higher-order spectral (HOS) methods are proving beneficial to improved understanding of nonlinear aeroelastic phenomena. Higher-order spectral methods enable the visualization of the transfer of energy from one frequency to another, a hallmark of nonlinear phenomena that is not visible using traditional spectral methods.

The paper is organized as follows. A description of HOS methods is provided, including two illustrative examples. A description of the NATA and a MATLAB model of the NATA then are provided, including the equations of motion that define the dynamics of the system. Application of HOS methods to aeroelastic transients from the NATA model are then presented. This is followed by a description of the F-18 flight flutter test data and analysis of the data using HOS methods.

Higher-Order Spectra

The primary benefit of higher-order spectra (HOS), also known as higher-order frequency response functions, is that they provide information regarding the transfer of energy among frequencies due to a nonlinear process. For example, bispectra have been used in the study of grid-generated turbulence to identify the nonlinear exchange of energy from one frequency to another (related to the turbulent cascade phenomenon). Linear concepts, by definition, cannot provide this type of information. In addition, higher-order spectra are the frequency-domain version of the Volterra series. For details regarding this relationship, the reader is referred to the recent article by Silva.¹³ Some very interesting and fundamental applications using the frequency-domain Volterra theory^{14,15} and experimental applications of Volterra methods^{16,17} are providing new “windows” on the world of nonlinear aeroelasticity.

In the recent work by Hajj and Silva,^{18,19} the aerodynamic and structural aspects of the flutter phenomenon of a wind-tunnel model are determined via a frequency domain analysis based on a hierarchy of spectral moments. The power spectrum is used to determine the distribution of power among the frequency components in the pressure, strain and acceleration data. The cross-power spectrum, linear coherence, and phase relation of the same frequency components between different signals are used to characterize the bending and torsion characteristics of the model. The nonlinear aspects of the aerodynamic loading are determined from estimates of higher-order spectral moments, namely, the auto- and cross-bispectrum.

For a discrete, stationary, real-valued, zero-mean process, the auto-bispectrum is estimated as²⁰

$$\hat{B}_{xxx}[l_1, l_2] = \frac{1}{M} \sum_{k=1}^M X_T^{(k)}[l_1 + l_2] X_T^{*(k)}[l_1] X_T^{*(k)}[l_2] \quad (1)$$

where $X_T^{(k)}[l]$ is the Discrete Fourier Transform of the k^{th} ensemble of the time series $x(t)$ taken over a time, T , and M is the number of these ensembles. The auto-bispectrum of a signal is a two-dimensional function of frequency and is generally complex-valued. In averaging over many ensembles, the magnitude of the auto-bispectrum will be determined by the presence (or absence) of a phase relationship among sets of the frequency components at l_1 , l_2 , and $l_1 + l_2$. If there is a random phase relationship among these three components, the auto-bispectrum will average to a very small value. Should a phase relationship exist among these frequency components, the corresponding auto-bispectrum will have a large magnitude.²¹ Because a quadratic nonlinear interaction between two frequency components, l_1 and l_2 , yields a phase relation between them and their summed component, $l_1 + l_2$, the auto-bispectrum can be used to detect a quadratic coupling or interaction among different frequency components of a signal. The level of such coupling in a signal can then be associated with a normalized quantity of the auto-bispectrum, called the auto-bicoherence, and defined as

$$b_{xxx}^2[l_1, l_2] = \frac{|\hat{B}_{xxx}[l_1, l_2]|^2}{\frac{1}{M} \sum_{k=1}^M |X_T^{(k)}[l_1] X_T^{(k)}[l_2]|^2 \frac{1}{M} \sum_{k=1}^M |X_T^{(k)}[l_1 + l_2]|^2} \quad (2)$$

By the Schwarz inequality, the value of $b_{xxx}^2[l_1, l_2]$ varies between zero and one. If no phase relationship exists among the frequency components at l_1 , l_2 , and $l_1 + l_2$, the value of the auto-bicoherence will be at or

near zero (due to averaging effects). If a phase relationship does exist among the frequency components at l_1 , l_2 , and $l_1 + l_2$, then the value of the auto-bicoherence will be at or near unity. Values of the auto-bicoherence between zero and one indicate partial quadratic coupling.

For systems where multiple signals are considered, detection of nonlinearities can be achieved by using the cross-spectral moments. For two signals $x(t)$ and $y(t)$, their cross-bispectrum is estimated as

$$\hat{B}_{yxx}[l_1, l_2] = \frac{1}{M} \sum_{k=1}^M Y_T^{(k)}[l_1 + l_2] X_T^{*(k)}[l_1] X_T^{*(k)}[l_2] \quad (3)$$

where $X_T^{(k)}[l]$ and $Y_T^{(k)}[l]$ are the Discrete Fourier Transforms of the k^{th} ensemble of the time series $x(t)$ and $y(t)$, respectively, over a time, T . The cross-bispectrum provides a measure of the nonlinear relationship amongst the frequency components at l_1 and l_2 in $x(t)$ and their summed frequency component, $l_1 + l_2$, in $y(t)$. Similar to the auto-bispectrum, the cross-bispectrum of signals $x(t)$ and $y(t)$ is a two-dimensional function in frequency and is generally complex-valued. In averaging over many ensembles, the magnitude of the cross-bispectrum will also be determined by the presence, or absence, of a phase relationship among sets of the frequency components at l_1 , l_2 , and $l_1 + l_2$. If there is a random phase relationship among the three components, the cross-bispectrum will average to a very small value. Should a phase relationship exist amongst these frequency components, the corresponding cross-bispectral value will have a large magnitude. The cross-bispectrum is then able to detect nonlinear phase coupling among different frequency components in two signals because of its phase-preserving effect.

Similarly to defining the auto-bicoherence, one can define a normalized cross-bispectrum to quantify the level of quadratic coupling in two signals. This normalized value is called the cross-bicoherence and is defined as

$$b_{yxx}^2[l_1, l_2] = \frac{|\hat{B}_{yxx}[l_1, l_2]|^2}{\frac{1}{M} \sum_{k=1}^M |X_T^{(k)}[l_1] X_T^{(k)}[l_2]|^2 \frac{1}{M} \sum_{k=1}^M |Y_T^{(k)}[l_1 + l_2]|^2} \quad (4)$$

If no phase relationship exists amongst the frequency components at l_1 , l_2 in $x(t)$ and the frequency component at $l_1 + l_2$ in $y(t)$, the value of the cross-bicoherence will be at or near zero. If a phase relationship does exist amongst these frequency components, the value of the cross-bicoherence will be at or near unity. Values of cross-bicoherence between zero and one indicate partial quadratic coupling. A digital procedure for computing the auto and cross-bicoherence is given by Kim and Powers²⁰ and is summarized by Hajj et al.²²

An important property of HOS functions involves the Gaussianity of a signal. The auto-bicoherence of a Gaussian signal is identically zero. This is an important theoretical result that is described in the literature. In addition, it is well-known that if a Gaussian signal is input to a linear system, then the output will be Gaussian as well. Therefore, computation of the auto-bicoherence for a Gaussian output will yield a value at or near zero, indicative of a linear process. If a Gaussian signal is applied to a nonlinear system, the output will be non-Gaussian. As a result, the auto-bicoherence for the output of the nonlinear system will yield a non-zero value. This characteristic of HOS methods can be exploited to identify regions where the behavior is transitioning from linear to nonlinear dynamics.

First Example

Using a linear (Eq. 5) and a nonlinear (van der Pol oscillator, Eq. 6) differential equation, the effect of nonlinear processes on input Gaussian distributions can be demonstrated. A Gaussian signal is input to the linear and nonlinear differential equations. The histogram of the response for each system (linear and nonlinear) to the Gaussian input signal is presented in the following figures.

$$\dot{y}_1 = y_2, \dot{y}_2 = -y_2 - y_1 + input \quad (5)$$

$$\dot{y}_1 = y_2, \dot{y}_2 = \mu(1 - y_1^2)y_2 - y_1 + input \quad (6)$$

Presented in Figure 1 are the input and output histograms for the linear system. As can be seen, the linear system preserves the Gaussianity of the input signal. Presented in Figure 2 are the input and output

histograms for the nonlinear system. For the nonlinear case, the Gaussianity of the input signal has not been preserved and has, instead, been transformed into a non-Gaussian distribution radically different from the input distribution. This is a well-known characteristic of nonlinear systems. It is worthwhile to mention that the response of the van der Pol oscillator (the nonlinear ODE) is a limit cycle oscillation (LCO). It appears that the distribution for other LCO phenomena may have a similar structure.

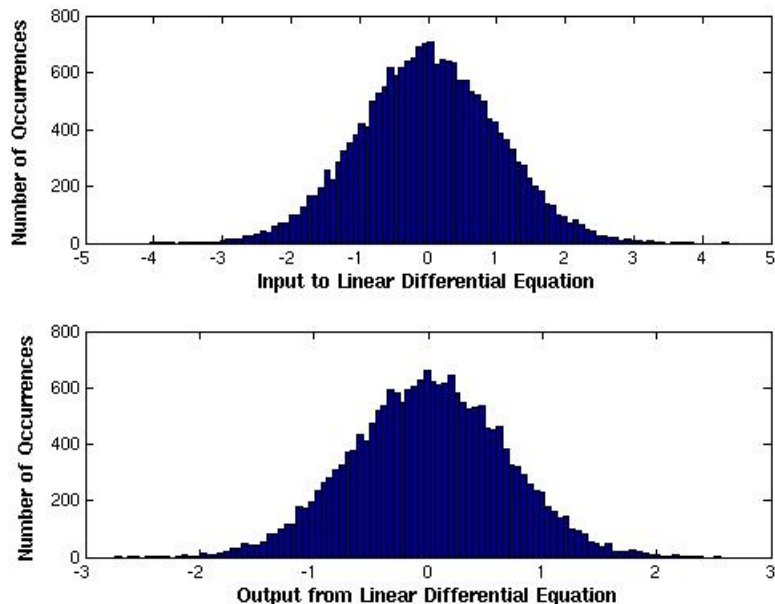


Figure 1. Histograms of the input and output for the linear system due to a Gaussian input.

HOS methods are very sensitive to variations in Gaussianity and, as will be shown, are valuable in identifying deviations from Gaussian behavior. Deviations from Gaussian behavior, as shown above, indicate the existence of a nonlinear process.

Second Example

A simple example is now presented in order to explain some of the concepts associated with HOS methods. The example²³ consists of a linear (y) and a nonlinear (z) time series, both with added Gaussian noise (d). The equations for these time series are

$$x(k) = \sin(2\pi(f_1)k + \frac{\pi}{3}) + \sin(2\pi(f_2)k + \frac{\pi}{8}) \tag{7}$$

$$y(k) = x(k) + d(k) \tag{8}$$

$$z(k) = x(k) + 0.05x^2(k) + d(k) \tag{9}$$

where $f_1 = 0.12$ Hz and $f_2 = 0.30$ Hz.

Figures 3 and 4 each contain the time series and the associated magnitude of the Fourier transforms for the linear and nonlinear time series, respectively. The dominant frequencies (in this case 0.12 and 0.30 Hz) are clearly visible in both figures. The frequency content for the nonlinear time series indicates the existence of additional frequencies. The nature of these frequencies, whether or not these frequencies are random or the result of a nonlinear coupling process, cannot be discerned from this analysis.

The power spectrum densities (PSD) for the linear and nonlinear time series are presented as Figure 5. Here again, the existence of additional frequencies in the PSD of the nonlinear time series (as compared to

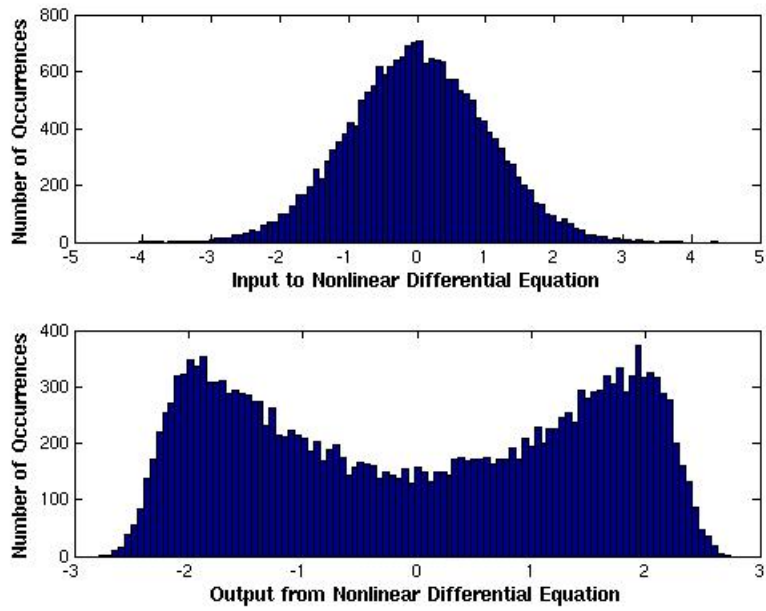


Figure 2. Histograms of the input and output for the nonlinear system due to a Gaussian input.

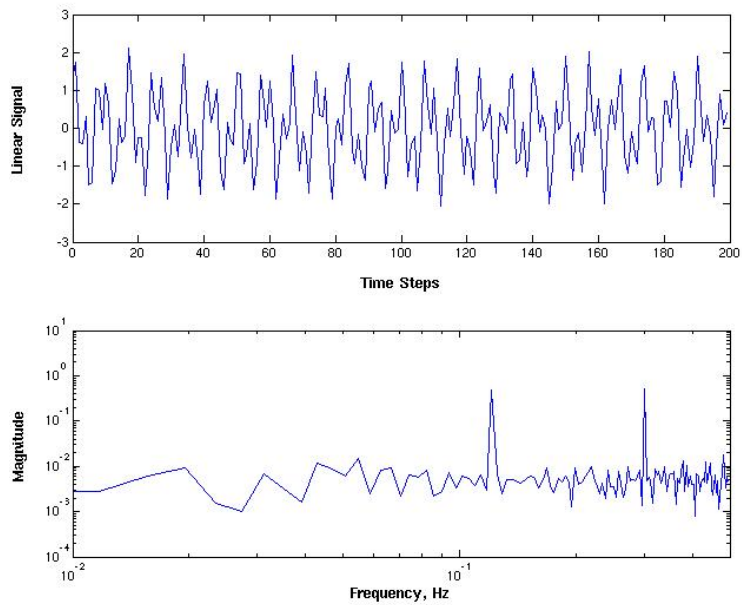


Figure 3. Linear time series and magnitude of frequency response.

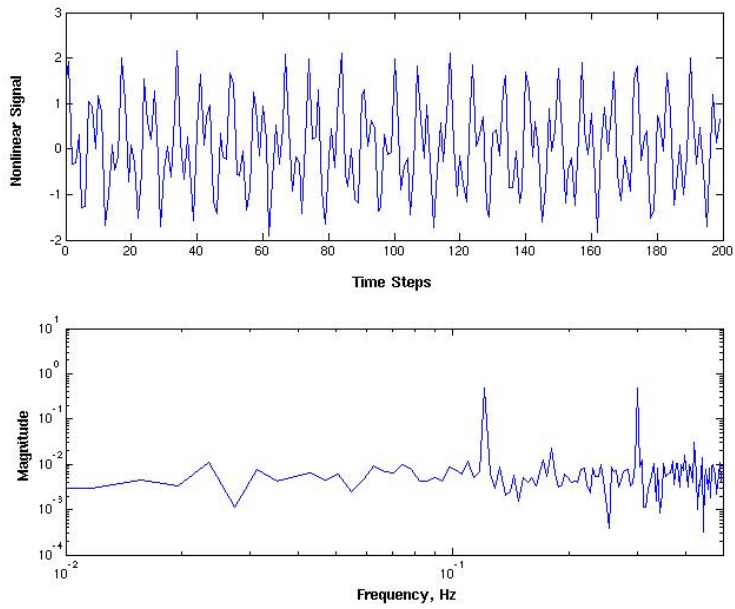


Figure 4. Nonlinear time series and magnitude of frequency response.

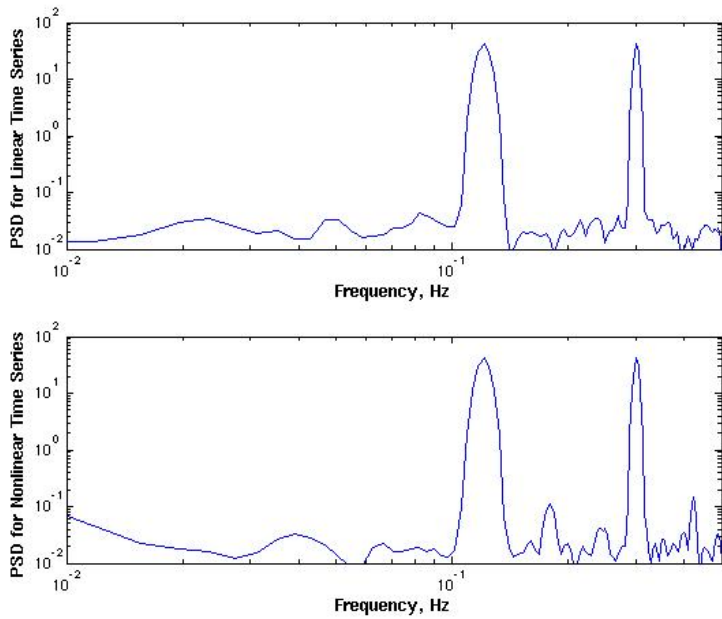


Figure 5. Power spectrum density (PSD) functions for linear and nonlinear time series.

the linear time series) is obvious. However, the PSD information cannot be used to discern if these additional frequencies are random or the result of a nonlinear coupling process.

In order to determine if these additional frequencies are random or the result of a nonlinear coupling process, the HOS for these time series must be computed. The magnitude of the bicoherence function for the linear time series, y , is presented as figure 6. The two frequency axes correspond to the two frequency indices in Eq. 2. If a significant peak is observed, this implies that the sum of those two frequencies is the result of a quadratic (nonlinear) coupling. It can be seen that the magnitude of the bicoherence function for the linear time series is quite low in value (compared to unity) and that there exist no dominant peaks that would be indicative of a nonlinear coupling.

The magnitude of the bicoherence function for the nonlinear time series is presented as Figure 7. In contrast to the bicoherence function for the linear time series, the bicoherence function for the nonlinear time series has several peaks at or close to unity, indicative of nonlinear (quadratic) coupling at the x - and y -axis frequencies indicated.

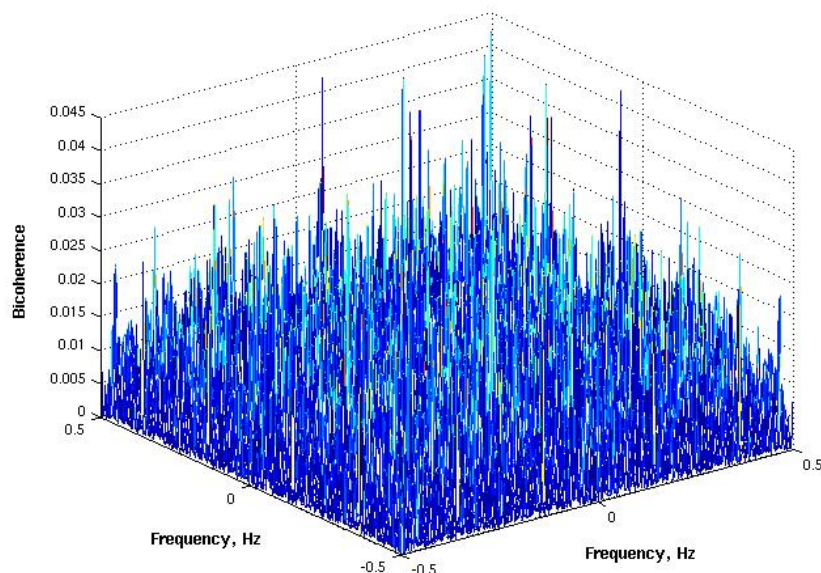


Figure 6. Bicoherence function for the linear time series.

Typically, in order to enhance visualization and interpretation of bicoherence functions, contour plots are viewed. The contour plot for Figure 7 is presented as Figure 8. The contour plot presents the frequencies that have coupled quadratically to generate the new frequencies that were visible in the PSD functions. In addition, the symmetry associated with the computation of the bicoherence function is also evident in the contour plot. The bicoherence function basically computes the correlation between two frequencies and the sum of those two frequencies. Therefore, for example, the bicoherence function for the first frequency (x -axis) being 2 Hz and the second frequency (y -axis) being 5 Hz will be the same as the bicoherence for the first frequency being 5 Hz and the second frequency being 2 Hz since their sum is the same.

This symmetry is presented in Figure 9. As Figure 9 indicates, knowledge of Region I (two such regions in the first quadrant) and Region II (two such regions in the fourth quadrant) is sufficient to completely define the remainder of the quadrants due to symmetry considerations. Regions I and II indicate that the original frequencies have been quadratically-coupled, resulting in new frequencies that are the sum (positive and negative) of the original frequencies. The new frequencies include 0.18, 0.24, and 0.42. The limitation of Region I to the triangle shown is due to the fact that the summation of two frequencies cannot exceed the Nyquist frequency (0.5, in this case). Therefore, the combination of the second frequency (0.30 Hz) with itself is not included since 0.60 Hz would be greater than the Nyquist frequency.

For subsequent results, although the bicoherence function is computed for all frequencies (positive and

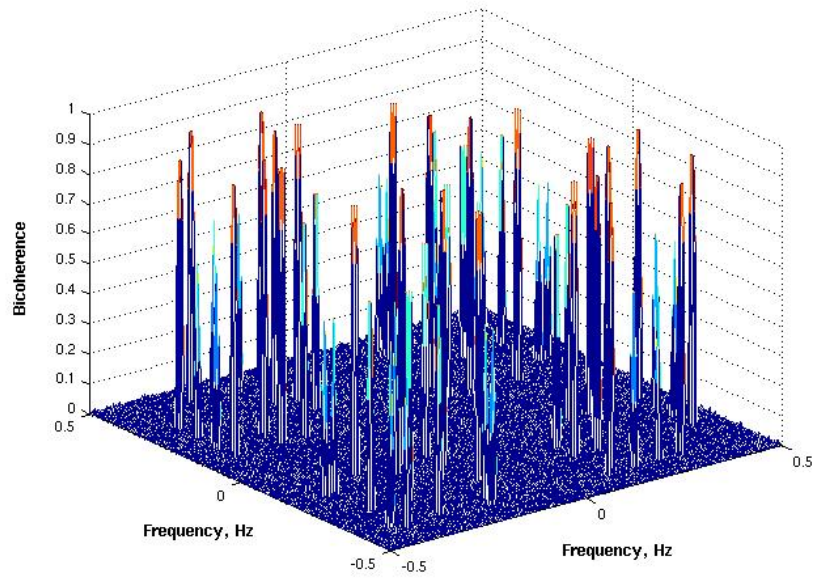


Figure 7. Bicoherence function for the nonlinear time series.

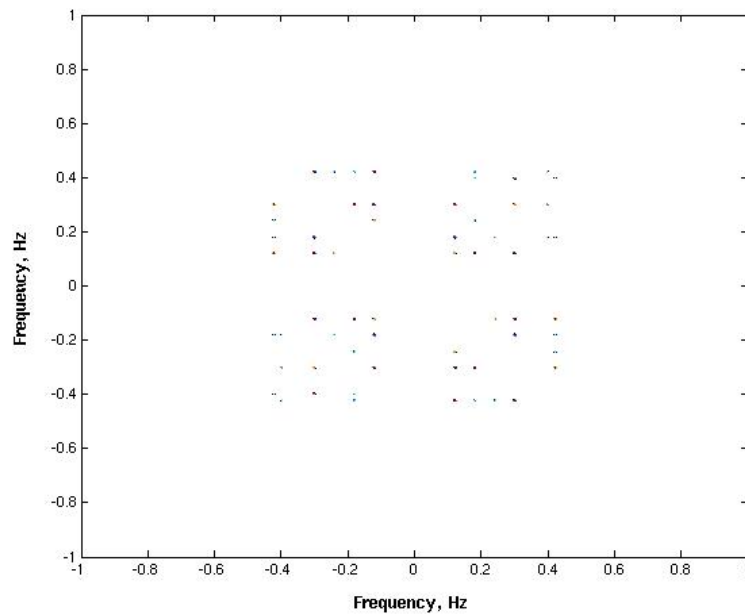


Figure 8. Contour plot of the bicoherence function for the nonlinear time series.

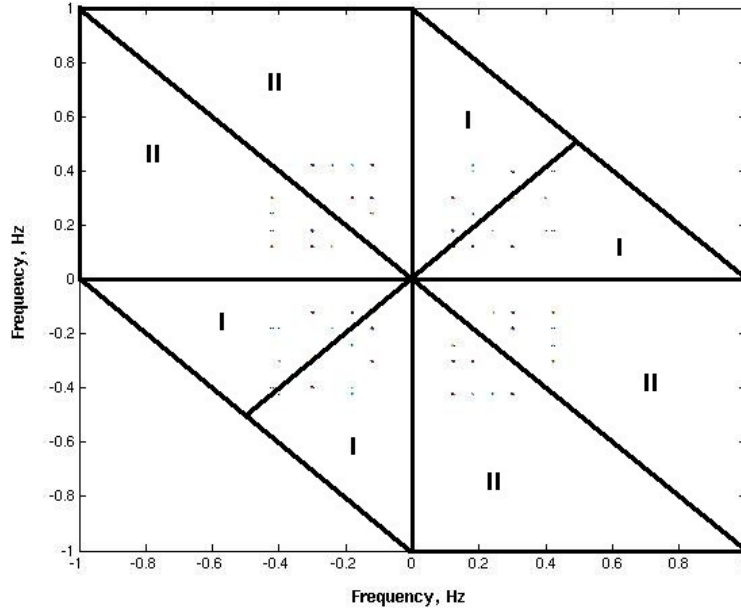


Figure 9. Contour plot of the bicoherence function for the nonlinear time series with symmetry regions identified.

negative), Region I in the first quadrant will be of primary interest for the sake of simplicity. This will be sufficient to demonstrate the applicability and value of HOS methods to flight flutter data.

Nonlinear Aeroelastic Testbed Apparatus (NATA)

The NATA in the Texas A&M University’s 2 ft. x 3 ft. Low Speed Wind Tunnel is used to generate free and controlled, linear and nonlinear aeroelastic transients at various conditions. Based on a simple two-degree-of-freedom concept with structurally nonlinear components, a rigid wing mounted on the NATA can exhibit nonlinear aeroelastic behavior, including LCO phenomena. The pitch and plunge motions of the NATA are enabled by springs that can be tuned to a wide variety of nonlinear stiffness characteristics. The NATA is shown in Figure 10.

A rigid wing attached to the NATA, as it would be mounted in the Low Speed Wind Tunnel, is shown in Figure 11. The nonlinear structural response is governed by a pair of cams that can be tuned to model various types of polynomial stiffness functions. Additional details regarding the NATA are available in the references.⁴⁻⁸

Analytical Model of NATA

A MATLAB model of the NATA/rigid wing system was generated and is briefly discussed in this section. The equations of motion for the system are presented as Eq. 10

$$\begin{bmatrix} m_T & m_w x_\alpha b \\ m_w x_\alpha b & I_\alpha \end{bmatrix} \begin{Bmatrix} \ddot{h} \\ \ddot{\alpha} \end{Bmatrix} + \begin{bmatrix} c_h & 0 \\ 0 & c_\alpha \end{bmatrix} \begin{Bmatrix} \dot{h} \\ \dot{\alpha} \end{Bmatrix} + \begin{bmatrix} k_h & 0 \\ 0 & k_\alpha(\alpha) \end{bmatrix} \begin{Bmatrix} h \\ \alpha \end{Bmatrix} = \begin{Bmatrix} -L \\ M \end{Bmatrix} \quad (10)$$

where

- m_T total mass (wing and NATA)
- m_w mass of the wing
- x_α static unbalance

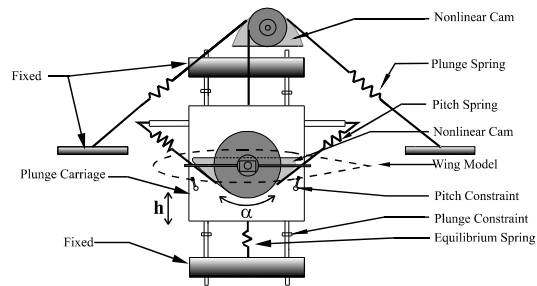


Figure 10. Schematic of the Nonlinear Aeroelastic Testbed Apparatus (NATA).

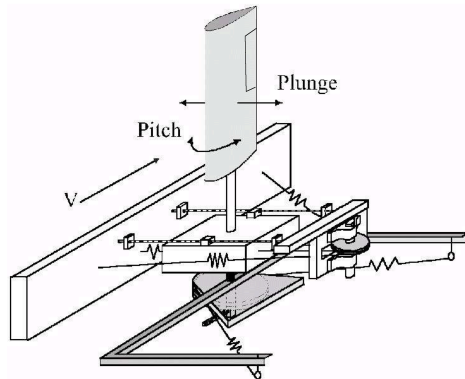


Figure 11. Schematic of the Nonlinear Aeroelastic Testbed Apparatus (NATA) with rigid airfoil and control surface.

b	semichord
I_α	mass moment of inertia about the elastic axis
h	plunge degree of freedom
α	pitch degree of freedom
c_h	plunge damping coefficient
c_α	pitch damping coefficient
k_h	plunge stiffness coefficient
k_α	pitch stiffness coefficient
L	lift
M	moment

The lift (L) and moment (M) on the right-hand side of Eq. 10 are defined using quasi-steady aerodynamics as presented in Eq. 11 and Eq. 12.

$$L = \rho U^2 b c_{l\alpha} \left(\alpha + \frac{\dot{h}}{U} + \left(\frac{1}{2} - a \right) b \frac{\dot{\alpha}}{U} \right) + \rho U^2 b c_{l\beta} \beta \quad (11)$$

$$M = \rho U^2 b^2 c_{m\alpha} \left(\alpha + \frac{\dot{h}}{U} + \left(\frac{1}{2} - a \right) b \frac{\dot{\alpha}}{U} \right) + \rho U^2 b^2 c_{m\beta} \beta \quad (12)$$

where

ρ	density
U	freestream velocity
$c_{l\alpha}$	lift due to angle of attack
$c_{l\beta}$	lift due to control surface deflection
β	control surface deflection
$c_{m\alpha}$	moment due to angle of attack
$c_{m\beta}$	moment due to control surface deflection

Results for the NATA

In this section, aeroelastic transients that range from a stable response to an LCO response, generated in MATLAB using the analytical model of the NATA, are presented. Then, in order to investigate the level of nonlinearity for each transient, Gaussian inputs will be applied to the system via the control surface. The output responses will be analyzed for their level of Gaussianity. Deviations from a Gaussian distribution can be interpreted as deviations from linear behavior. The auto-bicoherence is also presented to demonstrate the ability of HOS methods to discern Gaussianity from non-Gaussianity. For simplicity, the results presented are limited to the pitch motion.

Figure 12 presents the aeroelastic transient in pitch for a condition where a stable aeroelastic response is generated at a small velocity ($U=5$ m/sec) with small initial conditions as perturbations and no control surface input. The aeroelastic transient is clearly stable and the frequencies of the system are evident in the plot of the magnitude of the frequency response function of the pitch motion.

Figure 13 presents the aeroelastic transient in pitch for a condition where an LCO has been reached at a velocity of $U=20$ m/sec. The frequency content is exhibiting greater complexity than the previous aeroelastic transient.

To determine the level of nonlinearity that may be present starting from the stable transient ($U=5$ m/sec) all the way to the LCO transient ($U=20$ m/sec), a Gaussian input is applied via the control surface and the resulting nature of the output transient (Gaussian or non-Gaussian) is determined. This approach serves to demonstrate the sensitivity of HOS methods to non-Gaussian signals.

A Gaussian input is generated and applied to the aeroelastic system via the control surface. The histogram of the input is presented as Figure 14, where the Gaussian nature of the signal is evident. The auto-bicoherence for the Gaussian input is presented as Figure 15. The small values of the auto-bicoherence for the Gaussian input are as expected for a signal with a Gaussian distribution.

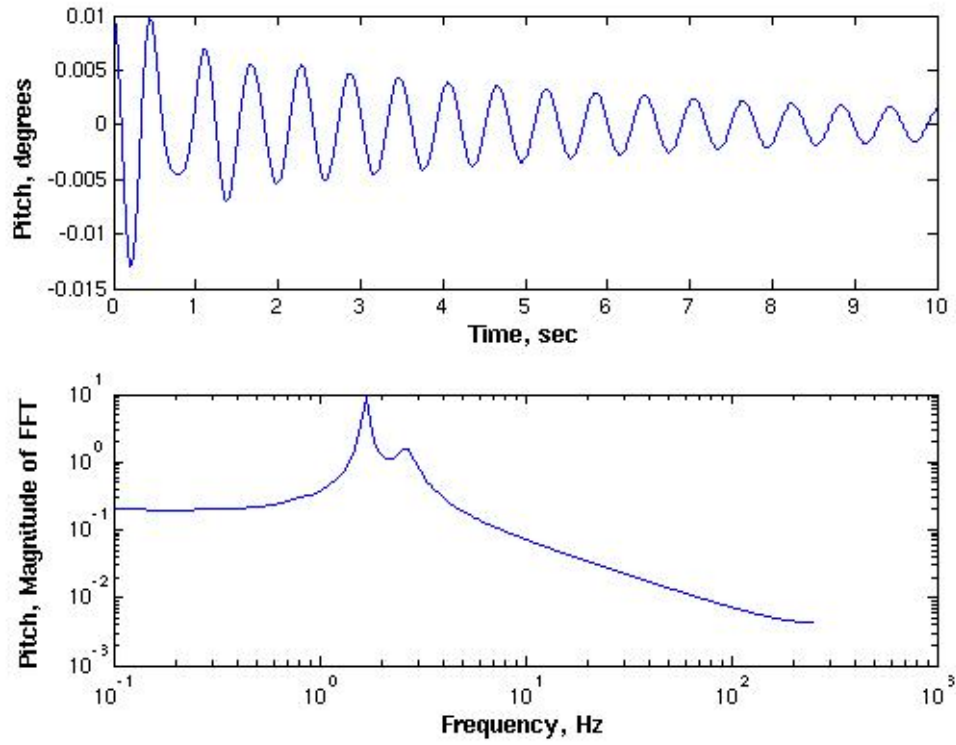


Figure 12. Stable aeroelastic response in pitch at $U=5$ m/sec: Time domain and frequency domain.

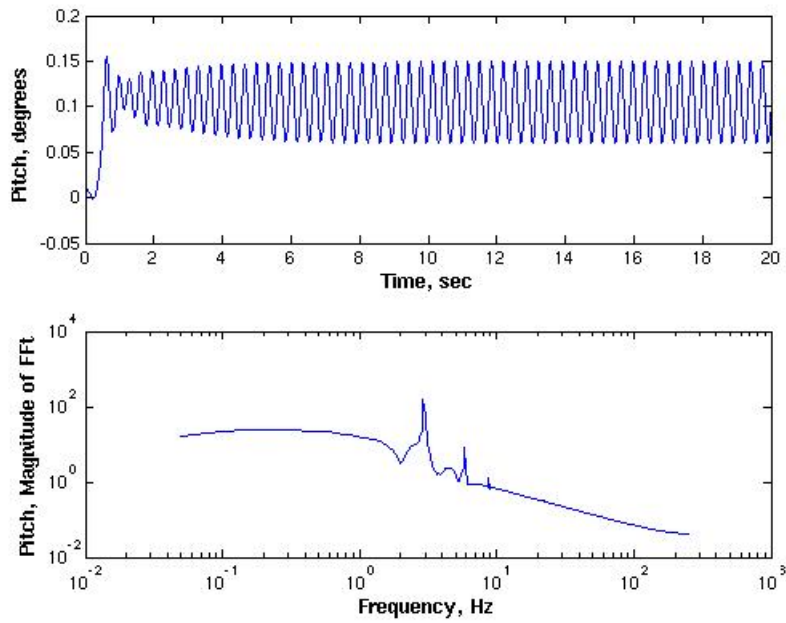


Figure 13. Limit cycle oscillation (LCO) aeroelastic response in pitch at $U=20$ m/sec: Time and frequency domain.

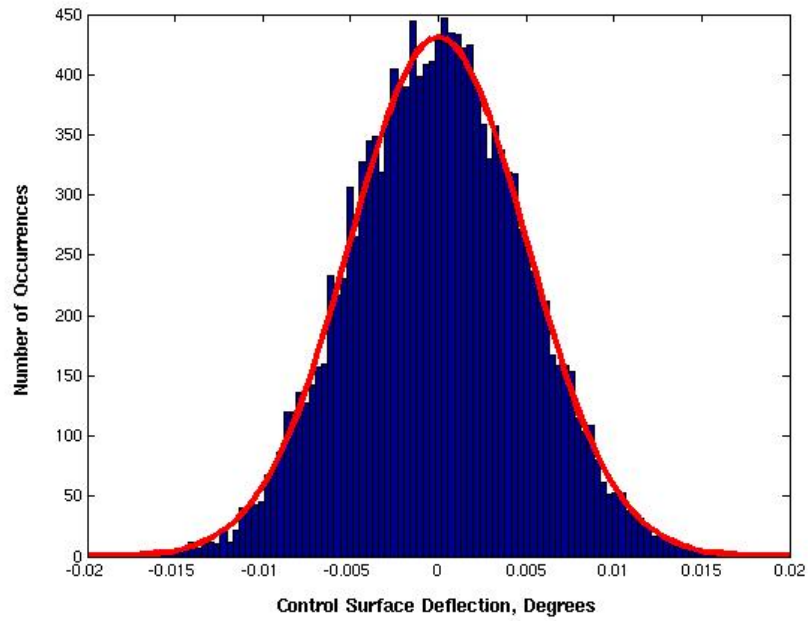


Figure 14. Histogram of the Gaussian input and theoretical Gaussian distribution (red).

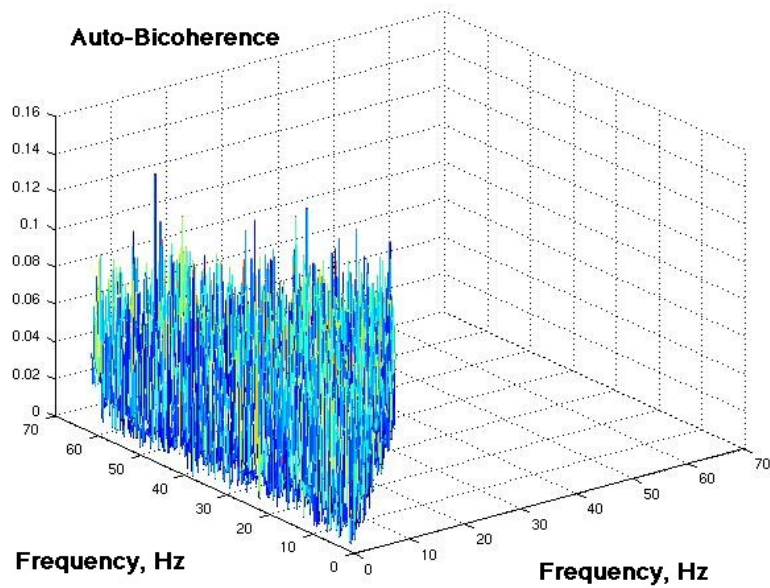


Figure 15. Auto-bicoherence of the Gaussian control surface input.

The resultant aeroelastic response (at $U=5$ m/sec) and the corresponding magnitude of the frequency response are presented in Figure 16. The effect of the Gaussian input is evident in the transient as well as the frequency content when Figure 16 is compared with Figure 12. However, neither of these two functions can be used to indicate the presence or level of any nonlinear interactions. The histogram of the output response (pitch, in this case) is presented as Figure 17.

The histogram for the output response indicates a noticeable deviation from the theoretical Gaussian distribution, indicating that the Gaussian input has been processed through some level of nonlinear interactions.

The auto-bicoherence for this aeroelastic response, presented as Figure 18, confirms the existence of nonlinear coupling at frequencies close to the LCO frequency (3 Hz).

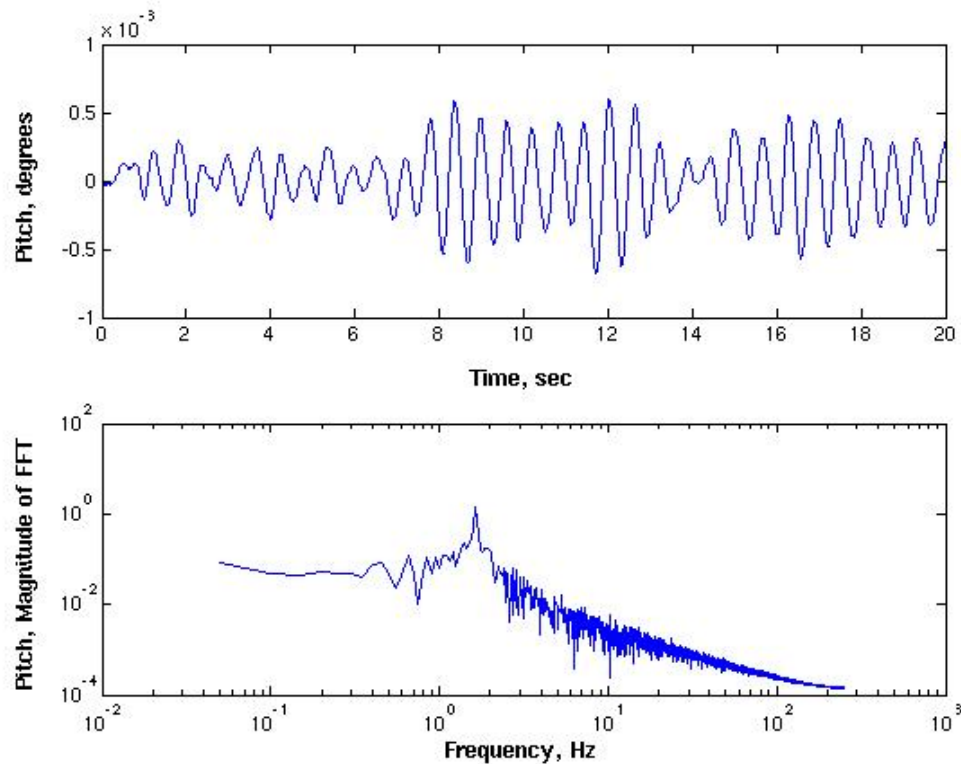


Figure 16. Stable aeroelastic response in pitch at $U=5$ m/sec with Gaussian control surface input: Time and frequency domain.

The velocity is increased to $U=10$ m/sec and the same Gaussian input is applied. The aeroelastic response, along with the magnitude of the frequency response, is presented in Figure 19.

Once again, the information presented in Figure 19 cannot be used to discern if any nonlinear interactions are taking place at this condition. However, the histogram of the output, presented as Figure 20, indicates an increased level of deviation from Gaussianity.

The auto-bicoherence for this condition is presented as Figure 21, with increasing levels of nonlinear interaction near the frequency of the LCO. The important point to be made is that both, the histograms and the auto-bicoherence, are indicating the presence of nonlinear phenomena prior to the visible onset of the LCO at $U=20$ m/sec.

The same Gaussian control surface input was applied for the $U=20$ m/sec condition at which LCO is encountered. The resulting LCO aeroelastic transient and the corresponding magnitude of the frequency response in pitch for that conditions is presented as Figure 22. The histogram of the pitch response is presented as Figure 23, where the deviation from Gaussianity is obvious. The resulting histogram of the LCO pitch response is clearly non-Gaussian with a bi-modal character, similar to the histogram generated from the output of the van der Pol equation. Figure 24 presents the corresponding aut-bicoherence for this

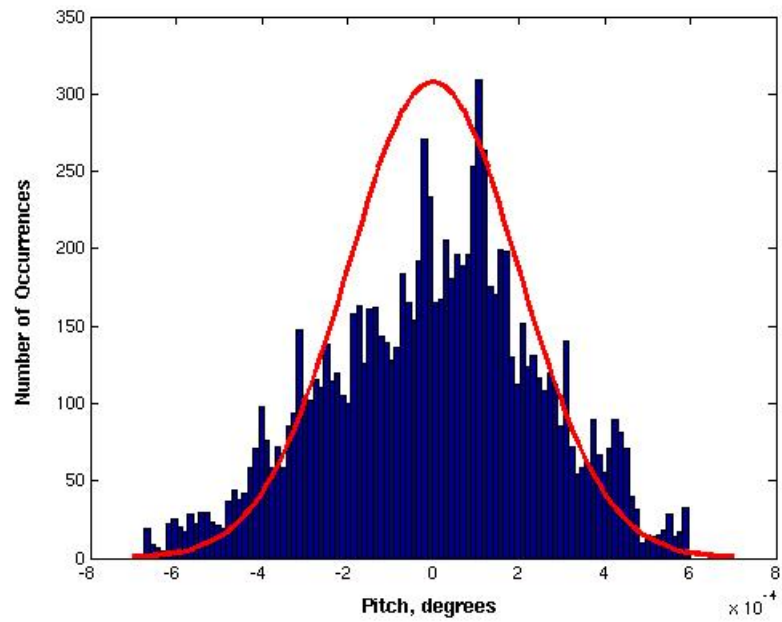


Figure 17. Histogram of stable aeroelastic response in pitch at $U=5$ m/sec due to Gaussian control surface input.

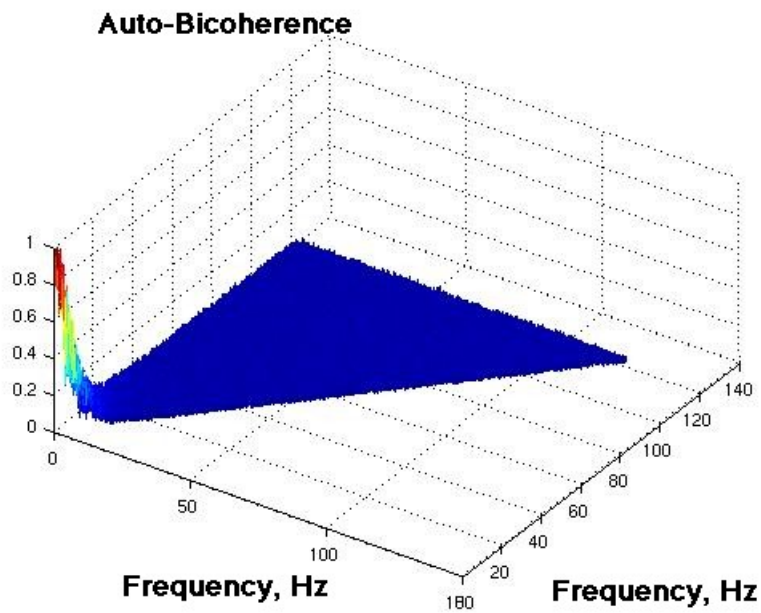


Figure 18. Auto-bicoherence of stable aeroelastic response in pitch at $U=5$ m/sec due to Gaussian control surface input.

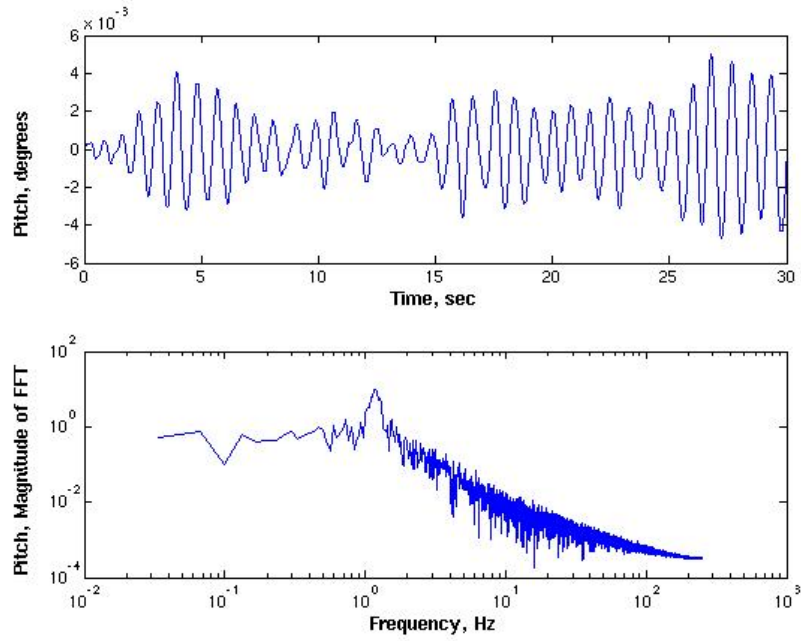


Figure 19. Stable aeroelastic response in pitch at $U=10$ m/sec with Gaussian control surface input: Time and frequency domain.

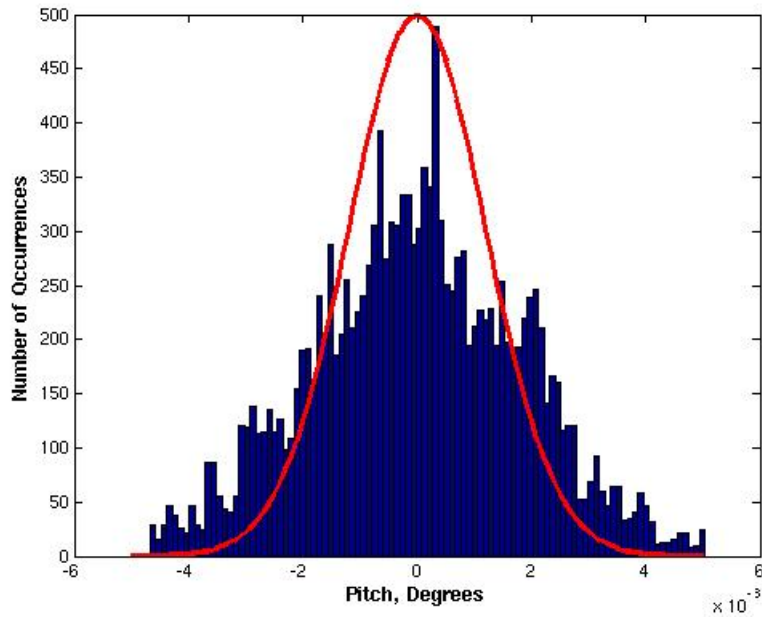


Figure 20. Histogram of stable aeroelastic response in pitch at $U=10$ m/sec due to Gaussian control surface input.

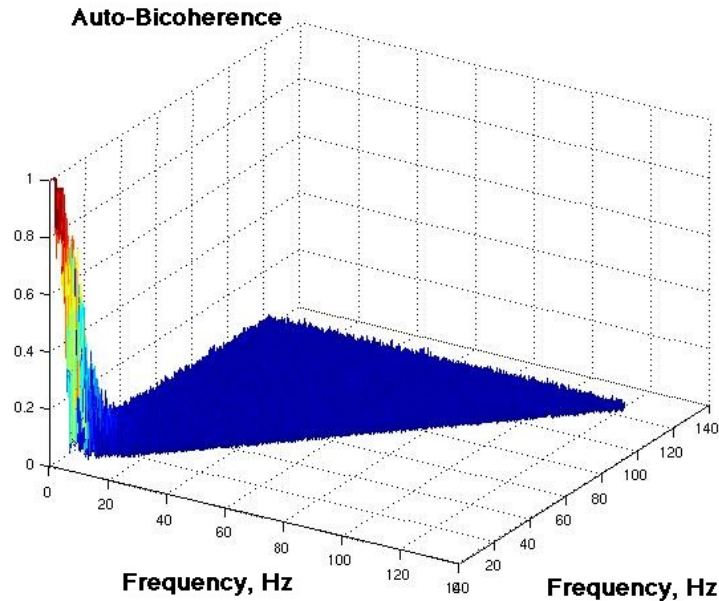


Figure 21. Auto-bicoherence of stable aeroelastic response in pitch at $U=10$ m/sec due to Gaussian control surface input.

condition. The auto-bicoherence for this LCO condition captures the nonlinear interactions that occur in the vicinity of the LCO frequency with greater resolution than the previous conditions.

Therefore, using this type of information (input/output histograms and auto-bicoherence) may enable the identification of precipitous nonlinear behavior prior to the actual onset during wind-tunnel or flight testing. This capability would provide greater insight into the testing process as well as enhanced insight regarding the nature of the nonlinear aeroelastic response.

F-18 Flight Flutter Test Data Description

A brief description of the Royal Australian Air Force (RAAF) F-18 flight flutter data is now provided. Additional details regarding the aircraft configuration and instrumentation is given in Arms et al.²⁴ and Keeler et al.²⁵

The aircraft's Antisymmetric Wing 1st Bending (AW1B) mode exhibits a large decrease in stiffness over a portion of the flight envelope. This nonlinear and temporary reduction in stiffness creates the illusion of a highly damped (i.e., stable) system. But when flying into another portion of the flight envelope, the wing's AW1B mode stiffness returns to its normal (linear) value and the aircraft may encounter an unsafe flutter condition.

Clearly, a strong motivation exists to develop methods that can identify regions of nonlinear behavior prior to their effects becoming significant. With this in mind, the present research effort has focused on the analysis of the flight flutter data using HOS methods in addition to the more traditional approaches.

A very large amount of data was acquired during these flight tests. Based on the signal-to-noise ratio of the data and the clearly identified data points, the data can be classified as high-quality data. This paper is not intended to be a comprehensive review of the data; some of the references listed above already serve that purpose. In addition, due to the sensitive nature of the data, only generic information (pre-LCO, for example) will be provided instead of the parameters of the flight condition such as Mach number and altitude.

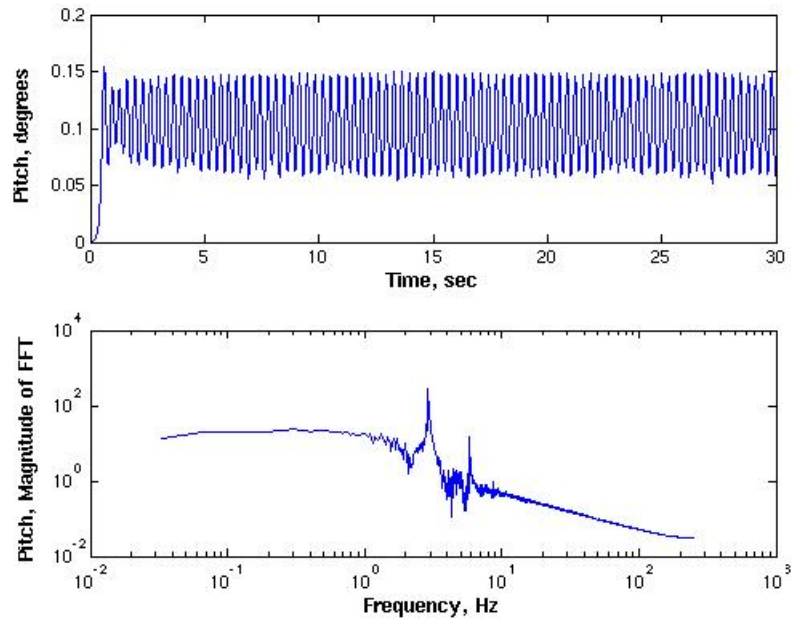


Figure 22. LCO aeroelastic response in pitch at $U=20$ m/sec with Gaussian control surface input: Time and frequency domain.

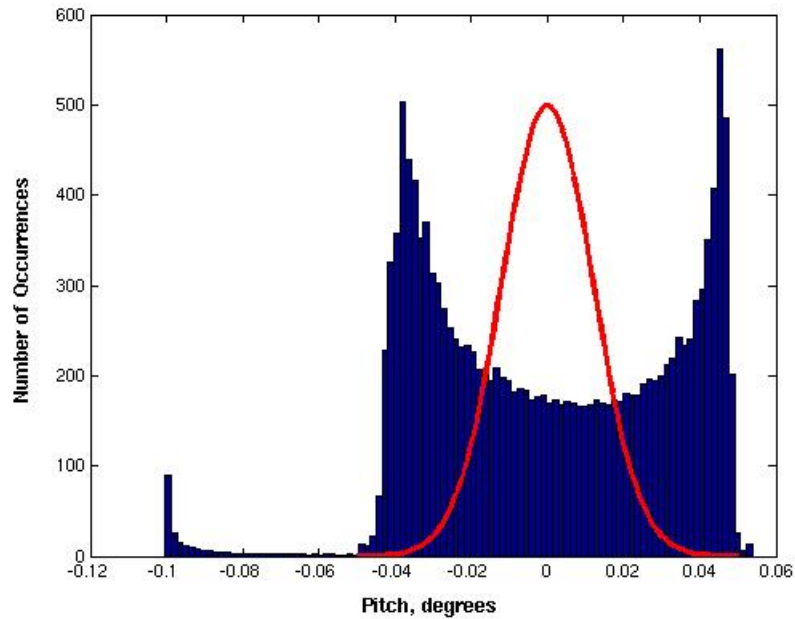


Figure 23. Histogram of LCO aeroelastic response in pitch at $U=20$ m/sec due to Gaussian control surface input.

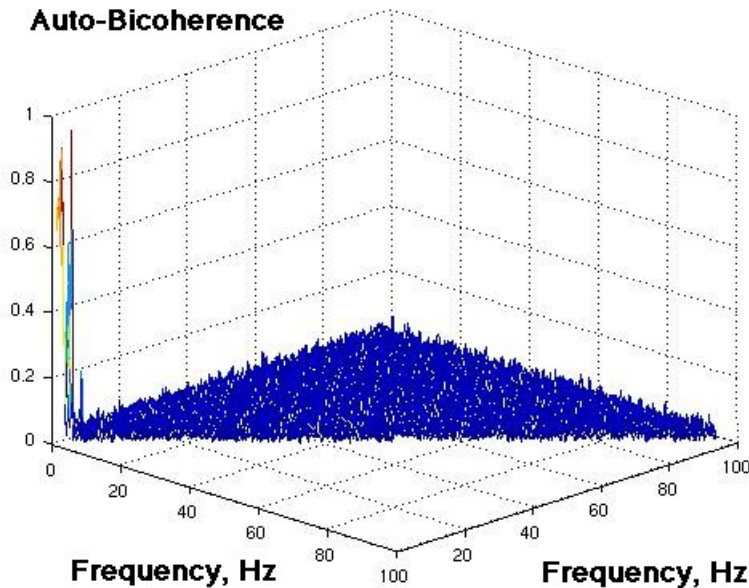


Figure 24. Auto-bicoherence of LCO aeroelastic response in pitch at $U=20$ m/sec due to Gaussian control surface input.

Results for the F-18 Flight Flutter Test Data

In this section, data analysis using traditional and HOS methods is presented. The data analyzed consists of data acquired using lateral stick raps. The lateral stick rap data represents data that was acquired as an LCO event was approached. The inputs (lateral stick raps) are in degrees of aileron motion and the outputs are accelerations at the forward launcher location (at the wing tip).

Lateral Stick Rap Input Data

Figure 25 presents a lateral stick rap input via the aileron and the resultant output acceleration measured at the forward launcher tip. At this condition, the aircraft does not exhibit any type of instability and basically returns to its original, undisturbed position.

The power spectrum density (PSD) plots for the lateral stick rap input and output and the linear coherence function for this input/output pair are presented as Figure 26.

As can be seen, the PSD of the output does not exhibit any noticeable differences from the PSD of the input, indicative of a predominantly linear situation. The linear coherence function indicates strong correlation (indicative of linear behavior) up to about 3 Hz, with subsequent peaks falling below unity (indicative of nonlinear behavior). A broad peak at around 5 Hz with a coherence of about 0.8 is present but with no significant peaks at this frequency in the PSD of the input and output, it is difficult to glean additional information from this plot.

In order to provide additional guidance regarding the linear or nonlinear nature of the current flight condition, the bicoherence of the output is generated. The output can be separated into two regions: the region prior to the application of the lateral stick rap input and the region after application of the lateral stick rap input. The bicoherence for the output data prior to the lateral stick rap input is presented as Figure 27. The small values of the bicoherence and the lack of any significant peaks supports the assertion that this flight condition is predominantly linear in nature.

The bicoherence for the output data after the lateral stick rap input is presented as figure 28. Although the values of the bicoherence are still low, there are some noticeable peaks that were not present in the previous figure. These peaks are in the region of the 5 Hz LCO phenomenon. This serves to illustrate

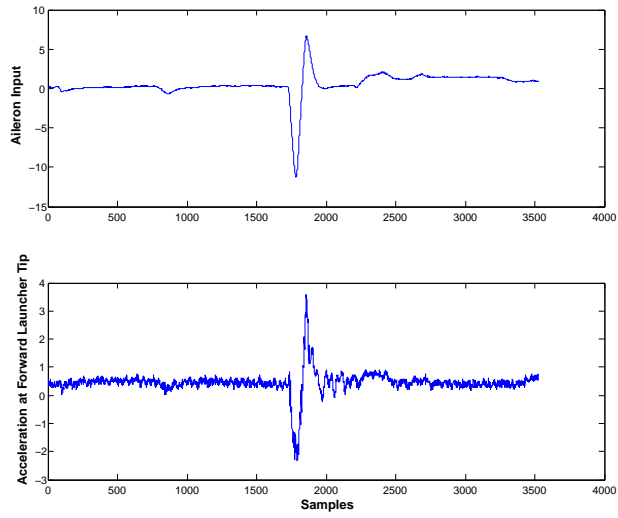


Figure 25. Lateral stick rap input and acceleration response for benign condition.

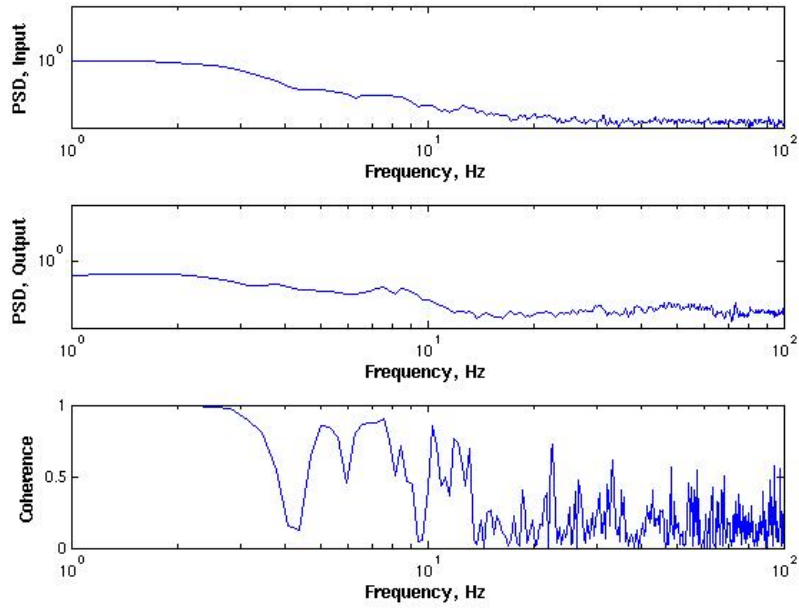


Figure 26. Power spectrum density plots for lateral stick rap input and acceleration output and linear coherence function for this input/output pair at benign flight condition.

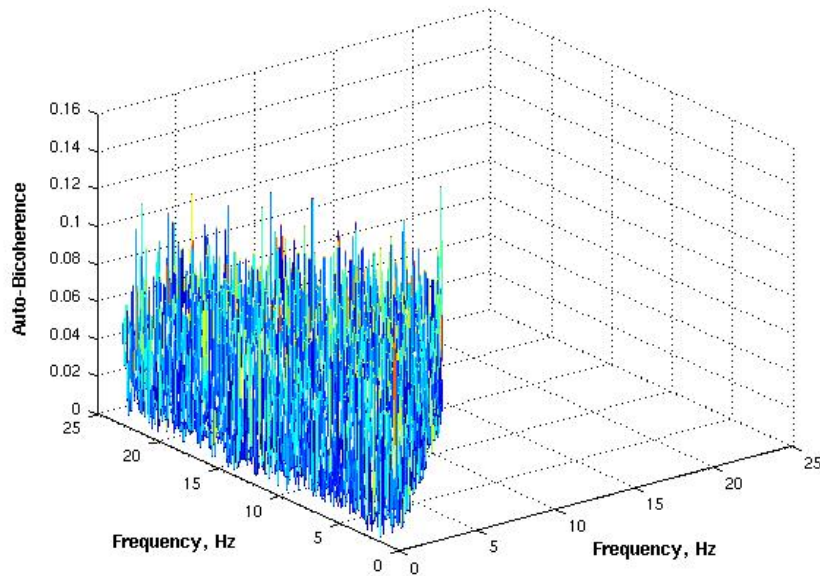


Figure 27. Auto-Bicoherence function for output data prior to lateral stick rap input at benign condition.

the high sensitivity of the HOS functions to identify potential nonlinear couplings at conditions that would appear benign using traditional methods.

Shown in figure 29 is the lateral stick rap input and acceleration response for a different flight condition. At this condition, it is clear that the input has excited the aircraft into an LCO event. The PSD of the input and output and the coherence function for this condition is presented as Figure 30. The PSD of the output reveals a strong peak at about 5.5 Hz, the LCO frequency. Since the coherence function indicates a very low value for this frequency, this implies that this frequency is not linearly correlated with the input (i.e, a nonlinear response).

The bicoherence function for the output data prior to the application of the lateral stick rap for this condition is presented as figure 31. The larger values displayed by this bicoherence function supports the increasing level of nonlinear interactions that are occurring at this flight condition. Based on this result, HOS methods may be suitable for identifying regions of nonlinear dynamics prior to the full onset of the nonlinear phenomena. It is interesting to note that the bicoherence function indicates that the approximate 8 Hz frequency (slightly noticeable in the PSD output plot for this condition) is the result of a nonlinear interaction.

Additional data analysis must be performed in order to verify the accuracy of results presented using HOS methods. Although HOS methods possess the necessary sensitivity to identify nonlinear coupling mechanisms, this sensitivity can also cause computational difficulties if caution is not exercised during computation of HOS functions.

In order to enhance the robustness of HOS methods, data manipulation techniques should be investigated to determine the optimal procedure for HOS analysis.

Conclusion

Simulated responses from a MATLAB model of the Texas A&M University's Nonlinear Aeroelastic Testbed Apparatus (NATA) with a rigid wing were presented. Aeroelastic transients generated included stable aeroelastic responses as well as nonlinear responses, or limit cycle oscillations (LCO). Higher-order spectra were computed and served to indicate the existence of nonlinear interactions prior to the LCO event. Data from RAAF F/A-18 flight flutter tests was presented and analyzed using traditional and higher-order

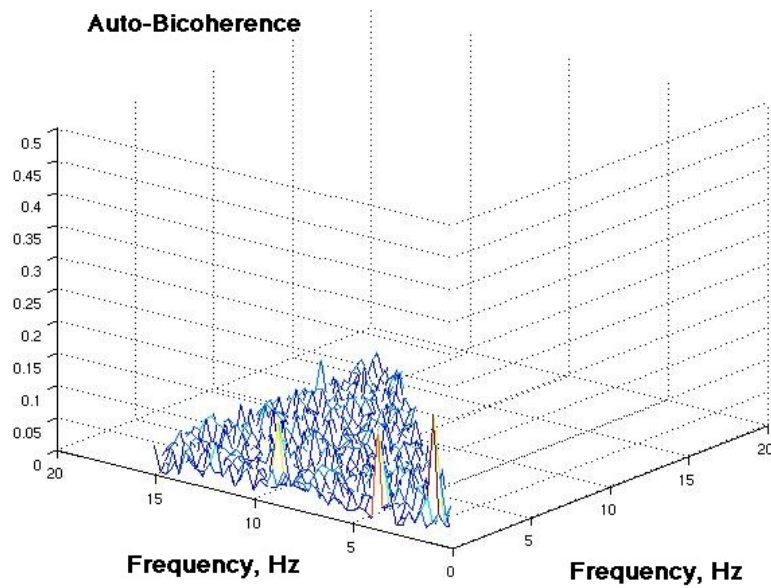


Figure 28. Auto-Bicoherence function for output data after lateral stick rap input at benign condition.

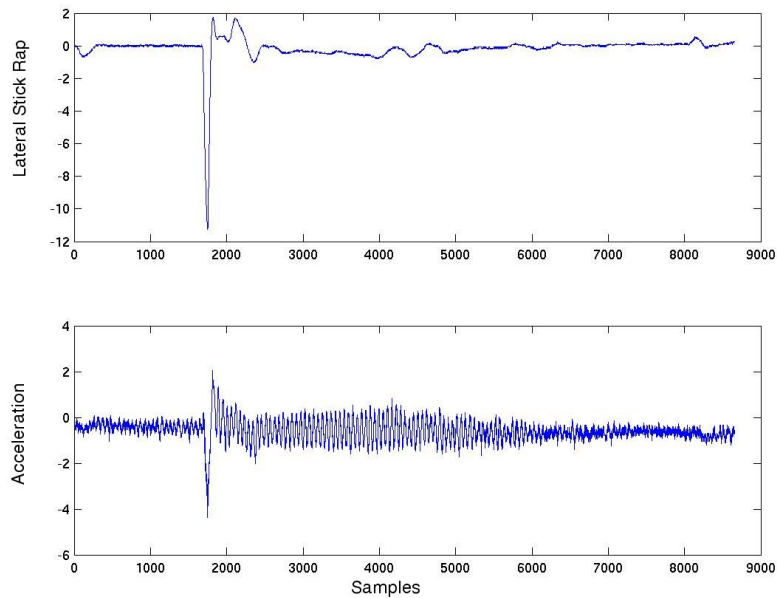


Figure 29. Lateral stick rap input and acceleration response at flight condition where an LCO is encountered.

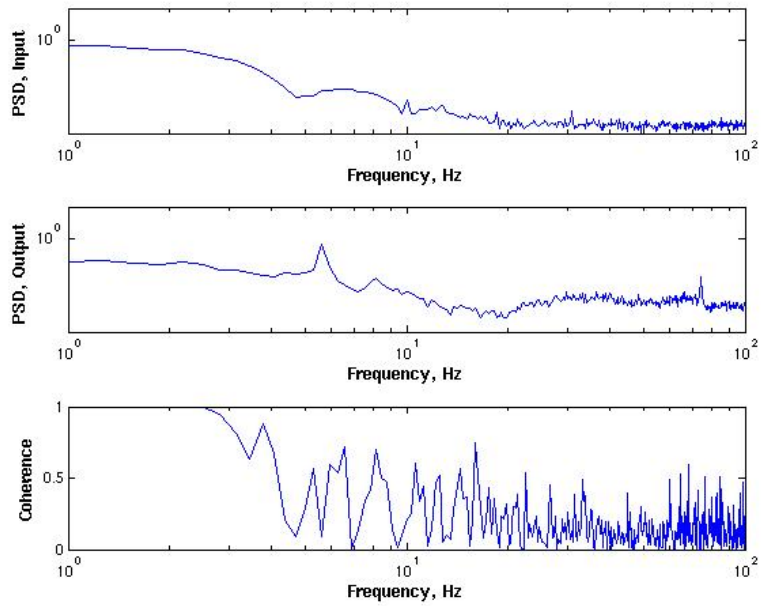


Figure 30. Power spectrum density plots for lateral stick rap input and acceleration output and linear coherence function for this input/output pair at flight condition where LCO was encountered.

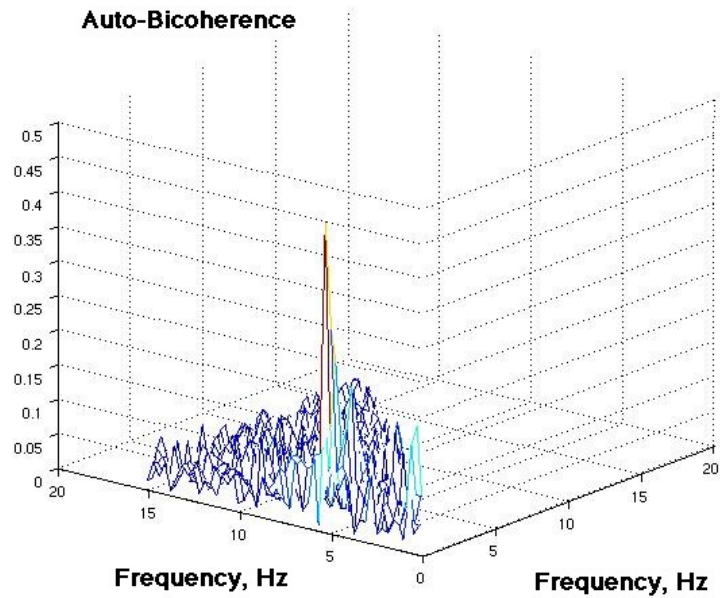


Figure 31. Auto-Bicoherence function for output data prior to lateral stick rap input at LCO condition.

spectral techniques. The high-quality data, which includes flutter and LCO phenomena, is well-suited for the application of higher-order spectral methods that can be used to detect nonlinearities in experimental measurements. Higher-order spectral analyses, primarily bicoherence functions, were generated at different flight conditions in order to understand the transition from linear to nonlinear aeroelastic behavior, including LCO phenomena. Additional research is underway to perform additional HOS data analyses in order to determine a preferred process for the routine application of HOS methods to flight test data.

Acknowledgments

The first author would like to acknowledge the support of NASA Langley's Office of Education and its support of the first author's research via the Floyd L. Thompson Fellowship. In addition, the support and education provided by Prof. Hajj (Virginia Tech) and Profs. Powers and Stearman (U. of Texas, Austin) during the first author's Fellowship is greatly acknowledged.

References

- ¹Dowell, E. H., Edwards, J. W., and Strganac, T., "Nonlinear Aeroelasticity," *Journal of Aircraft*, Vol. 40, Sept. 2003, pp. 857–874.
- ²Dunn, S. A., Farrell, P. A., Budd, P. J., Arms, P. B., Hardie, C. A., and Rendo, C. J., "F/A-18A Flight Flutter Testing-Limit Cycle Oscillation or Flutter?" *International Forum on Aeroelasticity and Structural Dynamics*, No. 00-2401, Madrid, Spain, June 2001.
- ³Denegri, C. M., "Limit Cycle Oscillation Flight Test Results of a Fighter with External Stores," *Journal of Aircraft*, Vol. 37, June 2001, pp. 761–769.
- ⁴O'Neill, T. G., "Experimental and Analytical Investigations of an Aeroelastic Structure with Continuous Nonlinear Stiffness," *PhD Thesis*, College Station, TX, May 1996.
- ⁵Block, J. J., "Active Control of an Aeroelastic Structure," *PhD Thesis*, College Station, TX, May 1996.
- ⁶Block, J. J. and Strganac, T. W., "Applied Active Control for a Nonlinear Aeroelastic Structure," *Journal of Guidance, Control, and Dynamics*, Vol. 21, 1998, pp. 838–845.
- ⁷Strganac, T. W., Ko, J., Thompson, D. E., and Kurdila, A. J., "Investigations of Limit Cycle Oscillations in Aeroelastic Systems," *International Forum on Aeroelasticity and Structural Dynamics*, jun 1999.
- ⁸Strganac, T. W., Ko, J., and Thompson, D. E., "Identification and Control of Limit Cycle Oscillations in Aeroelastic Systems," *Journal of Guidance, Control, and Dynamics*, Vol. 23, jun 2000, pp. 1127–1133.
- ⁹Thompson, D., "Nonlinear Analysis of Store-Induced Limit Cycle Oscillations," *PhD Thesis*, College Station, TX, Aug. 2001.
- ¹⁰Silva, W. A., Strganac, T. W., and Hajj, M. R., "Higher-Order Spectral Analysis of a Nonlinear Pitch and Plunge Apparatus," *46th AIAA/ASME/ASCE/AHS/ASC Structures, Structural Dynamics, and Materials Conference*, No. 2005-2013, April 2005.
- ¹¹Hajj, M. R. and Silva, W. A., "Nonlinear Flutter Aspects of the Flexible High-Speed Civil Transport Semispan Model," *Journal of Aircraft*, Vol. 41, 2004, pp. 1202–1208.
- ¹²Silva, W. A. and Dunn, S., "Higher-Order Spectral Analysis of F-18 Flight Flutter Data," *46th AIAA/ASME/ASCE/AHS/ASC Structures, Structural Dynamics, and Materials Conference*, No. 2005-2014, April 2005.
- ¹³Silva, W. A., "Identification of Nonlinear Aeroelastic Systems Based on the Volterra Theory: Progress and Opportunities," *Journal of Nonlinear Dynamics*, Vol. 39, Jan. 2005.
- ¹⁴Marzocca, P., Librescu, L., and Silva, W. A., "Nonlinear Stability and Response of Lifting Surfaces via Volterra Series," *presented at the 20th International Congress of Theoretical and Applied Mechanics, Chicago, IL, 27 August - 2 September 2000*.
- ¹⁵Marzocca, P., Librescu, L., and Silva, W. A., "Volterra Series Approach for Nonlinear Aeroelastic Response of 2-D Lifting Surfaces," *presented at the 42nd Structures, Structural Dynamics, and Materials Conference, 16-19 April 2001, Seattle, WA, 16-19 April 2001*.
- ¹⁶Kurdila, A. J., Carrol, B., Nishida, T., and Sheplak, M., "Reduced-Order Modeling for Low Reynolds Number Flow Control," *SPIE Conference on Mathematics and Control in Smart Structures, Newport Beach, CA*, Vol. 3667, March 1999, pp. 68–79.
- ¹⁷Praznica, R., Kurdila, A., and Silva, W. A., "Multiresolution Methods for Representation of Volterra Series and Dynamical Systems," *AIAA Paper 2000-1754*, April 2000.
- ¹⁸Hajj, M. R. and Silva, W. A., "Nonlinear Flutter Aspects of the Flexible HSCT Semispan Model," *Proceedings of the 44th Structures, Structural Dynamics and Materials Conference*, No. 2003-1515, Norfolk, VA, April 2003.
- ¹⁹Hajj, M. R. and Silva, W. A., "Nonlinear Flutter Aspects of the Flexible HSCT Semispan Model," *International Forum on Aeroelasticity and Structural Dynamics*, No. US-39, Amsterdam, The Netherlands, 4-6 June 2003.
- ²⁰Kim, Y. C. and Powers, E. J., "Digital Bispectral Analysis and its Applications to Nonlinear Wave Interactions," *IEEE Transactions of Plasma Science*, Vol. PS-7, 1979, pp. 120–131.
- ²¹Hajj, M. R., Miksad, R. W., and Powers, E. J., "Fundamental Subharmonic Interaction: Effect of the Phase Relation," *Journal of Fluid Mechanics*, 1993.

²²Hajj, M. R., Miksad, R. W., and Powers, E. J., "Perspective: Measurements and Analyses of Nonlinear Wave Interactions with Higher-Order Spectral Moments," *Journal of Fluid Engineering*, 1997.

²³Choudhury, M. A. A. S., Shah, S. L., and Thornhill, N. F., "Detection and Diagnosis of System Nonlinearities Using Higher Order Statistics," *15th Triennial IFAC World Congress*, Barcelona, Spain, 2002.

²⁴Arms, P., Farrell, P., and Dunn, S., "AF/A-18 ASRAAM Flutter Flight Testing - The Aussie Approach," *Society of Experimental Test Pilots Symposium*, Los Angeles, CA, Sept. 2000.

²⁵Keeler, A., Arms, P., Farrell, P., and Dunn, S., "AF/A-18 / AIM-132 ASRAAM and AIM-9 Sidewinder Flutter Testing," *Aircraft Stores Compatibility Symposium*, Florida, March 2001.